Dnase1l3 deletion causes aberrations in length and end-motif frequencies in plasma DNA

Lee Serpas, Rebecca W y Chan, Peiyong Jiang, Meng Ni, Kun Sun, Ali Rashidfarrokhi, Chetna Soni, Vanja Sisirak, Wing-Shan Lee, Suk Hang Cheng, et al.

Dnase1l3 deletion causes aberrations in length and end-motif frequencies in plasma DNA

Lee Serpas[a,1], Rebecca W. Y. Chan[b,c,1], Peiyong Jiang[b,c], Meng Ni[b,c], Kun Sun[b,c], Ali Rashidfarrokhi[a], Chetna Soni[a], Vanja Sisirak[a,d], Wing-Shan Lee[b,c], Suk Hang Cheng[b,c], Wenlei Peng[b,c], K. C. Allen Chan[b,c], Rossa W. K. Chiu[b,c], Boris Reizis[a,2], and Y. M. Dennis Lo[b,c,2]

[a]Department of Pathology, New York University School of Medicine, New York, NY 10016; [b]Li Ka Shing Institute of Health Sciences, The Chinese University of Hong Kong, Shatin, NT, Hong Kong SAR, China; [c]Department of Chemical Pathology, Prince of Wales Hospital, The Chinese University of Hong Kong, Shatin, NT, Hong Kong SAR, China; and [d]UMR 5164 Immunologie Conceptuelle, Expérimentale et Translationnelle, ImmunoConcEpT, Université de Bordeaux, 33076 Bordeaux, France

Contributed by Y. M. Dennis Lo, November 23, 2018 (sent for review September 13, 2018; reviewed by Michael R. Speicher and Alain R. Thierry)

Circulating DNA in plasma consists of short DNA fragments. The biological processes generating such fragments are not well understood. DNASE1L3 is a secreted DNASE1-like nuclease capable of digesting DNA in chromatin, and its absence causes anti-DNA responses and autoimmunity in humans and mice. We found that the deletion of *Dnase1l3* in mice resulted in aberrations in the fragmentation of plasma DNA. Such aberrations included an increase in short DNA molecules below 120 bp, which was positively correlated with anti-DNA antibody levels. We also observed an increase in long, multinucleosomal DNA molecules and decreased frequencies of the most common end motifs found in plasma DNA. These aberrations were independent of anti-DNA response, suggesting that they represented a primary effect of DNASE1L3 loss. Pregnant *Dnase1l3*$^{-/-}$ mice carrying *Dnase1l3*$^{+/-}$ fetuses showed a partial restoration of normal frequencies of plasma DNA end motifs, suggesting that DNASE1L3 from *Dnase1l3*-proficient fetuses could enter maternal systemic circulation and affect both fetal and maternal DNA fragmentation in a systemic as well as local manner. However, the observed shortening of circulating fetal DNA relative to maternal DNA was not affected by the deletion of *Dnase1l3*. Collectively, our findings demonstrate that DNASE1L3 plays a role in circulating plasma DNA homeostasis by enhancing fragmentation and influencing end-motif frequencies. These results support a distinct role of DNASE1L3 as a regulator of the physical form and availability of cell-free DNA and may have important implications for the mechanism whereby this enzyme prevents autoimmunity.

liquid biopsy | cell-free DNA | noninvasive prenatal testing | systemic lupus erythematosus | cfDNA

There is much recent interest in the use of cell-free DNA in plasma for noninvasive prenatal testing (1, 2) and cancer liquid biopsies (3, 4). Circulating cell-free DNA molecules have a size distribution that suggests a nucleosomal origin (5, 6) and plasma DNA sequencing allows one to deduce information on gene expression-related nucleosome occupancy (7). Furthermore, circulating fetal-derived and tumor-derived DNA molecules have been shown to be shorter than the maternal and nontumoral counterparts, respectively (8–12). Plasma DNA size distribution analysis has been used for the noninvasive prenatal testing of fetal chromosomal aneuploidies (9, 13, 14). Enhanced detection of cancer-associated mutations in circulating DNA had been observed through the use of short PCR amplicons (15). Analysis of plasma DNA fragment size by paired-end sequencing had also contributed to improving cancer screening (16).

Biological factors that influence the size distribution of plasma DNA remain unknown. We had previously studied the size distribution of plasma DNA in mice with deletion of *Dnase1*, a well-studied mammalian extracellular nuclease (17). We did not observe any systematic change in plasma DNA size profile in this experimental model. However, plasma DNA molecules are essentially circulating fragmented nucleosomes, containing both DNA and histones. For its substrate, DNase1 preferentially digests naked DNA rather than chromatin (18). Hence, in retrospect, it is perhaps understandable that there is no clearly observable effect of deleting the *Dnase1* gene on the size profile of circulating DNA. Thus, there is a need to search for the possible role that other nucleases might play in determining the size profile of circulating DNA.

DNase1-like 3 (DNASE1L3), also referred to as DNase γ, is a member of a family of four extracellular nucleases homologous to DNASE1. DNASE1L3 and DNASE1 are jointly responsible for nearly all DNase activity in mammalian plasma (18). However, DNASE1L3 is more efficient at cleaving chromatin than DNASE1 (18, 19). In this work, we investigated whether deleting the *Dnase1l3* gene in mice would create aberrations of plasma DNA fragmentation patterns.

Significance

Circulating DNA in plasma has many diagnostic applications, including noninvasive prenatal testing and cancer liquid biopsy. Plasma DNA consists of short fragments of DNA. However, there is little information about mechanisms that are involved in the fragmentation of plasma DNA. We showed that mice in which *Dnase1l3* had been deleted showed aberrations in the fragmentation of plasma DNA. We also observed a change in the ranked frequencies of end motifs of plasma DNA caused by the *Dnase1l3* deletion. In *Dnase1l3*$^{-/-}$ mice pregnant with *Dnase1l3*$^{+/-}$ fetuses, we observed a partial reversal of the plasma DNA aberrations. This study has thus linked the fields of nuclease biology and circulating nucleic acids and has opened up avenues for future research.

Author contributions: Y.M.D.L. initiated the study; Y.M.D.L., R.W.Y.C., L.S., and B.R. designed research; L.S., R.W.Y.C., A.R., and S.H.C. performed research; P.J., M.N., K.S., W.L., and W.P. performed bioinformatics analysis; R.W.Y.C., P.J., K.S., K.C.A.C., R.W.K.C., B.R., and Y.M.D.L. analyzed data; L.S., A.R., C.S., V.S., and B.R. generated the gene-targeted mice; and R.W.Y.C., P.J., and Y.M.D.L. wrote the paper.

Reviewers: M.R.S., Medical University of Graz; and A.R.T., U896 INSERM, Institut Recherche en Cancérologie de Montpellier.

Conflict of interest statement: Y.M.D.L. is a scientific cofounder and a member of the scientific advisory board for Grail. Y.M.D.L., R.W.K.C., and K.C.A.C. hold equity in Grail and receive research funding from Grail/Cirina for other projects. Y.M.D.L., R.W.K.C., K.C.A.C., and P.J. are consultants to Grail. Y.M.D.L., R.W.K.C., and K.C.A.C. are cofounders and board members of DRA Company Limited. Y.M.D.L., R.W.Y.C., R.W.K.C., K.C.A.C., P.J., L.S., and B.R. plan to file a patent application based on the data generated from this work.

Data deposition: Sequence data for this work have been deposited in the European Genome-Phenome Archive (EGA), https://www.ebi.ac.uk/ega/, hosted by the European Bioinformatics Institute (accession no. EGAS00001003174).

[1]L.S. and R.W.Y.C. contributed equally to this work.

[2]To whom correspondence may be addressed. Email: Boris.Reizis@nyulangone.org or loym@cuhk.edu.hk.

This article contains supporting information online at www.pnas.org/lookup/suppl/doi:10.1073/pnas.1815031116/-/DCSupplemental.

Published online December 28, 2018.

Results

Size Profiling of Plasma DNA Using Electrophoresis. Mice with targeted *Dnase1l3* deletion were the primary focus of the present work. To test for potential genetic redundancy with *Dnase1*, we included mice with targeted *Dnase1* deletion as well as mice doubly deficient in *Dnase1* and *Dnase1l3*. *Dnase1l3*-deficient mice develop anti-DNA IgG antibodies and progressive systemic lupus erythematosus (SLE)-like disease (20), and we had previously demonstrated that human subjects with SLE had a variety of plasma DNA aberrations that were related to binding of anti-DNA antibodies to plasma DNA (21). As CD40 ligand (CD40LG) is important for mounting a humoral immune response (22, 23), we examined mice doubly deficient in DNASE1L3 and CD40LG to distinguish between the primary effects of DNASE1L3 deficiency and secondary effects of anti-DNA response in such mice.

SI Appendix, Fig. S1 shows the electrophoretic patterns of plasma DNA sequencing libraries prepared from WT mice and gene-targeted mice with different genotypes. The key observation was that *Dnase1l3* deletion was associated with increased prominence of the bands with mean peak values at 497 bp, 683 bp, and 906 bp (marked e, f, and g, respectively, in *SI Appendix*, Fig. S1). These signals, after deducting the length of the adaptor primers ligated to the DNA molecules (125 bp), correspond to di-, tri-, and tetranucleosomal sizes. A very weak dinucleosomal signal was observed for the WT mice and those with only the *Dnase1* gene deleted. No difference was observed between mice with just the *Dnase1l3* gene deleted and those in which *Dnase1l3* was deleted together with *Dnase1* or *Cd40lg*.

Sequencing of Plasma DNA. Paired-end sequencing was performed for the plasma DNA libraries from the WT mice and the four types of gene-targeted mice. Following DNA sequence alignment, the deletion of *Dnase1*, *Dnase1l3*, and *Cd40lg* genes for the respectively targeted mice could be observed (*SI Appendix*, Fig. S2).

Paired-end sequencing allowed the plasma DNA sizes to be determined at single-nucleotide resolution. Fig. 1*A* shows the overall size distribution of plasma DNA from the WT and four types of targeted mice. A peak frequency at ~165 bp was reminiscent of the nucleosomal nature of plasma DNA. Fig. 1*B* is a plot of the size distribution in which the *y* axis is plotted on a logarithmic scale so that the frequencies of the longer DNA fragments, which are a minority population, can be seen more clearly. Fig. 1*B* shows that *Dnase1l3* deletion is associated with an increase in the frequencies of plasma DNA molecules above 250 bp. Mice with *Dnase1* deletion did not show any notable difference in the frequencies of plasma DNA molecules above 250 bp compared with WT mice, as reported previously (17). Mice with only *Dnase1l3* deletion, those with *Dnase1l3*/*Dnase1* double deletion, and those with *Dnase1l3*/*Cd40lg* double deletion had similarly increased frequencies of plasma DNA molecules above 250 bp. The differences in the plasma DNA size profiles between the WT mice and mice with *Dnase1l3*$^{-/-}$ are illustrated in *SI Appendix*, Fig. S3. Fig. 2 indicates that *Dnase1l3* deletion, either alone or in combination with *Dnase1* or *Cd40lg* deletion, was associated with an increased percentage of plasma DNA molecules >250 bp. We observed a larger than twofold increase in the percentage of plasma DNA molecules of over 250 bp in mice with *Dnase1l3* deletion (median: 4.9%; range: 2.9–10.4%) compared with WT mice (median: 2.3%; range: 1.37–6.20%).

Fig. 1*C* shows the frequencies of relatively short plasma DNA molecules in the size range of 20–120 bp in the plasma of the WT and targeted mice. Notably, there was an increase in the frequencies of short plasma DNA molecules in the plasma of mice with *Dnase1l3* deletion, and those with double deletion of both *Dnase1l3* and *Dnase1*, compared with WT mice and those with *Dnase1* deletion or *Dnase1l3*/*Cd40lg* double deletion. In addition, we observed a 40% increase in the median percentage of plasma DNA molecules of less than 120 bp in mice with *Dnase1l3* deletion (median: 18.6%; range: 11.6–28.9%) compared with WT mice (median: 13.3%; range: 7.0–35.6%; *SI Appendix*, Fig. S4).

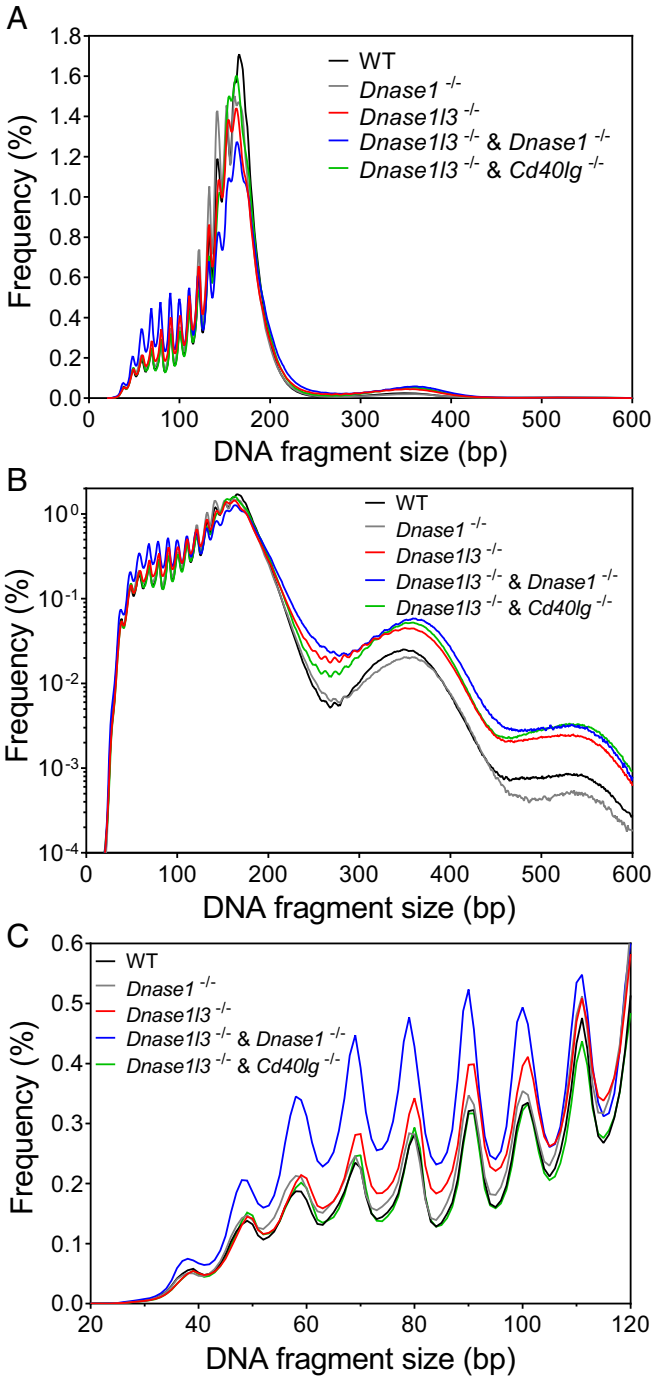

Fig. 1. Size distributions of plasma DNA fragments in the range from (*A*) 0–600 bp on linear scale, (*B*) 0–600 bp on logarithmic scale, and (*C*) 20–120 bp on linear scale. The mean size distribution for different groups is shown in different colors. The black, gray, red, blue, and green lines represent the average size profile of plasma DNA molecules originating from 9 WT mice, 3 mice with *Dnase1* deletion (*Dnase1*$^{-/-}$), 13 mice with *Dnase1l3* deletion (*Dnase1l3*$^{-/-}$), 2 mice with *Dnasell3* and *Dnase1* double deletion (*Dnasell3*$^{-/-}$ & *Dnase1*$^{-/-}$), and 5 mice with *Dnase1l3* and *Cd40lg* double deletion (*Dnasell3*$^{-/-}$ & *Cd40lg*$^{-/-}$), respectively.

In our previous work with human subjects with SLE, the presence of anti-DNA antibodies was associated with an increase

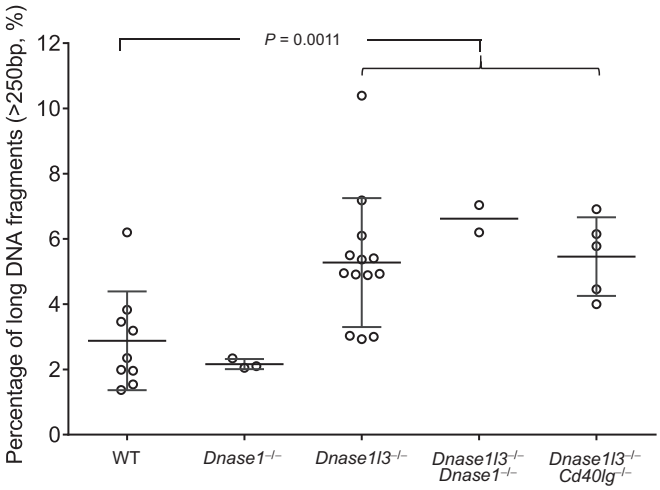

Fig. 2. Proportion of long plasma DNA fragments among groups. The proportion of long DNA fragments was determined from the percentage of sequenced reads with a size greater than 250 bp. Samples from 9 WT mice, 3 *Dnase1*$^{-/-}$ mice, 13 *Dnase1l3*$^{-/-}$ mice, 2 *Dnase1*$^{-/-}$/*Dnase1l3*$^{-/-}$ mice, and 5 *Dnaselll3*$^{-/-}$/*Cd40lg*$^{-/-}$ mice were sequenced. Each circle represents one mouse. Statistical difference in the percentage between WT mice and mice with *Dnase1l3* deletion was calculated by using the Wilcoxon rank-sum test.

in the frequencies of short plasma DNA molecules (21). We thus explored the correlation between the levels of anti-dsDNA antibody and the frequencies of short DNA molecules in the plasma of the studied mice. *SI Appendix*, Fig. S5*A* shows a positive correlation between the percentage of short plasma DNA molecules (≤120 bp) and the anti-dsDNA antibody levels (r = 0.5577, P = 0.0009, Spearman correlation). In contrast, we observed no correlation between the percentage of long plasma DNA molecules (>250 bp) and the anti-dsDNA antibody levels (*SI Appendix*, Fig. S5*B*; r = 0.0079, P = 0.9657, Spearman correlation). These results suggest that the increase in short DNA fragments may be caused by the anti-DNA response in *Dnase1l3*-deficient animals, whereas the increase in long DNA fragments may be a primary effect of DNASE1L3 deficiency.

The data in Figs. 1 and 2 were generated using the Illumina platform, which was designed for sequencing short reads and has a practical limit of readout at ∼600 bp. In view of this limitation, we also generated data using the single-molecule, real-time technology from Pacific Biosciences, which could generate sequencing data for molecules kilobases in length (24, 25). Using the platform from Pacific Biosciences, we further sequenced two plasma DNA libraries from each of the groups. We observed that plasma DNA molecules of 600 bp to 2,000 bp in size accounted for less than 4.8% of the circulating DNA molecules. *SI Appendix*, Fig. S6 shows data from the Pacific Biosciences platform and indicates that the proportion of long plasma DNA fragments in mice with *Dnase1l3* deletion is higher than that of the WT mice or mice with *Dnase1* deletion.

Frequency Distribution of Plasma DNA End Motifs and *Dnase1l3* Deletion. We next investigated if there might be DNA sequence motifs that would be preferentially cleaved by DNASE1L3. We reasoned that if DNASE1L3 contributed to the generation of plasma DNA fragments, then the preferred DNA sequence motifs would be present at high frequencies in the plasma of WT mice and reduced in the plasma of *Dnase1l3*$^{-/-}$ mice. Hence, we ranked the end motifs of plasma DNA in WT mice in descending order of frequencies (Dataset S1, tab "Wildtype"). Then, we removed from this ranked order any end motif that did not show significant reduction in the *Dnase1l3*$^{-/-}$ mice (Dataset S1, tab "Dnase1l3 del"). The top 25 end motifs that were found by such a procedure were all within the top 42 motifs defined in WT mice (Dataset S1), and are listed in Table 1. The top six motifs, CCCA, CCTG, CCAG, CCAA, CCAT, and CCTC, all started with CC and thus were considered together in subsequent analyses. These six motifs were all within the top eight motifs defined in WT mice, and together account for 7.43% (range: 6.05–8.10%) of plasma DNA ends in WT mice but only for 4.22% (range: 3.46–4.34%) in mice with *Dnase1l3* deletion. Fig. 3 shows the frequency of the combined percentages of the top six motifs in the plasma of WT mice and gene-targeted mice of different genotypes. We observed that *Dnase1l3* deletion was associated with a 45.3% reduction in the median frequency of these motifs compared with WT mice. Frequencies for each of the six motifs are shown in *SI Appendix*, Fig. S7 *A–F* and are consistent with the combined results shown in Fig. 3. Thus, the loss of DNASE1L3 reduced the frequencies of the most common sequence motifs of plasma DNA ends, suggesting that DNASE1L3 is primarily responsible for generating them in the steady state.

Size Profiling of Plasma DNA in Pregnant Mice. Plasma of a pregnant subject contains a mixture of DNA from the pregnant mother and her fetus(es) (1). By crossing female B6 mice with male BALB/c mice, the fetuses would have one half of their genomes with a B6 genetic background and the other half with a BALB/c background. Any DNA molecules in the plasma of the pregnant mothers that had a BALB/c genetic signature could be classified as fetal-derived.

Table 2 shows the characteristics of these pregnant mice. Fig. 4 shows the mean size profile of plasma DNA from two pregnant WT mice carrying WT fetuses, four *Dnase1l3*$^{-/-}$ pregnant mice carrying *Dnase1l3*$^{+/-}$ fetuses, and three *Dnase1l3*$^{-/-}$ pregnant mice carrying *Dnase1l3*$^{-/-}$ fetuses. An increase in the frequencies of relatively long plasma DNA molecules above 250 bp as well as an increase in the frequencies of relatively short plasma DNA molecules below 120 bp were observed in all *Dnase1l3*$^{-/-}$ pregnant mice irrespective of the fetal genotype. These characteristics are similar to those of plasma samples from nonpregnant mice (Fig. 1*B*).

We also sought to explore if differential size distributions between circulating fetal and maternal DNA molecules were still observable when the pregnant mother was deficient in DNASE1L3. Such analyses would also allow one to measure the percentage of fetal DNA in a particular maternal plasma sample (Table 2). However, circulating DNA molecules with genetic signatures of the B6 strain were predominantly, but not completely, of maternal origin. Fetal-derived DNA with genetic signatures of the B6 strain would be expected to comprise a small proportion of circulating DNA molecules as well.

Fig. 5*A* shows the size profile of BALB/c (i.e., fetal) and B6 (i.e., predominantly maternal) DNA in the plasma of a pregnant *Dnase1l3*$^{+/+}$ mouse carrying WT *Dnase1l3*$^{+/+}$ fetuses. As expected, the fetal DNA exhibited a relatively shorter size profile compared with that of the maternal DNA. *SI Appendix*, Fig. S8 shows that the percentage of fetal DNA below 150 bp (median: 32.8%; range: 20.5–40.6%) was lower than that of maternal DNA (median: 54.3%; range: 36.3–65.6%) in the pregnant murine plasma. Fig. 5*B* shows cumulative frequency plots of BALB/c and B6 DNA in maternal plasma. These cumulative frequency plots show the progressive accumulation of DNA molecules from the short to long ones. We further define a parameter, called ΔS, which represents the difference in the cumulative frequencies between the fetal and maternal DNA at a particular size (Fig. 5*B*). A positive value of ΔS for a particular size suggests that a larger amount of the fetal DNA molecules is present below that particular size compared with the maternal DNA molecules. Fig. 5*C* plots the difference in cumulative frequencies (ΔS) across different sizes between the BALB/c and B6 DNA in maternal plasma relative to DNA fragment size. ΔS peaks were observed at the nucleosomal (163 bp) and dinucleosomal (334 bp) sizes.

Table 1. Top 25 motifs with the highest frequency in WT mice and statistically significant reduction in *Dnase1l3*$^{-/-}$ mice

Motif	Motif frequency of WT, % (a)	Motif frequency of *Dnase1l3*$^{-/-}$, % (b)	Fold change (*a*/*b*)	*P* value
CCCA	1.51	0.76	1.98	<0.0001
CCTG	1.45	0.80	1.81	<0.0001
CCAG	1.37	0.56	2.47	<0.0001
CCAA	1.12	0.51	2.21	<0.0001
CCAT	1.11	0.67	1.66	<0.0001
CCTC	1.10	0.93	1.18	<0.0001
CAAA	1.02	0.78	1.32	<0.0001
TGTG	0.98	0.51	1.92	<0.0001
TGTT	0.96	0.58	1.65	<0.0001
CCTA	0.87	0.52	1.68	<0.0001
TATT	0.84	0.61	1.39	<0.0001
CCAC	0.81	0.45	1.81	<0.0001
TCTT	0.78	0.56	1.39	<0.0001
CCCC	0.77	0.54	1.44	<0.0001
TGAG	0.76	0.44	1.73	0.0001
CAAG	0.73	0.50	1.45	<0.0001
CATG	0.73	0.60	1.20	<0.0001
TATA	0.72	0.45	1.61	<0.0001
GGAA	0.68	0.55	1.25	<0.0001
TGTA	0.68	0.37	1.83	<0.0001
CATA	0.66	0.59	1.13	<0.0001
TACA	0.65	0.42	1.57	<0.0001
TCTG	0.65	0.45	1.45	<0.0001
CAAT	0.65	0.58	1.12	<0.0001
TGCT	0.64	0.41	1.57	0.0001

These results suggested that fetal DNA was present with a relatively higher proportion of fragments below 163 bp compared with the situation for maternal DNA. Furthermore, this difference between the size profiles of circulating fetal and maternal DNA was observed with or without *Dnase1l3* deletion.

Fig. 5 *D*–*F* show the size distribution, cumulative frequency, and ΔS plots for a pregnant *Dnase1l3*$^{-/-}$ mouse carrying *Dnase1l3*$^{+/-}$ fetuses. These plots were similar to those for pregnant WT (*Dnase1l3*$^{+/+}$) mice carrying WT (*Dnase1l3*$^{+/+}$) fetuses shown above. Hence, the shortening of circulating fetal DNA in maternal plasma was observed even in a pregnant mother that was *Dnase1l3*$^{-/-}$. The size difference between the maternal and fetal DNA of all other pregnant WT or *Dnase1l3*$^{-/-}$ mice is shown in *SI Appendix*, Fig. S9.

In this pregnancy model, when both the mothers and fetuses were of the B6 genetic background, one could identify the fetal DNA in the maternal plasma by analyzing DNA originating from the Y chromosome. As multiple fetuses were typically present in a murine pregnancy, there was a high probability that at least one of the fetuses would be male. *SI Appendix*, Fig. S10 shows the DNA size profiles of the Y chromosome (i.e., fetal) and autosomes (i.e., predominantly maternal) in the plasma of the pregnant WT (*Dnase1l3*$^{+/+}$) mice carrying WT (*Dnase1l3*$^{+/+}$) fetuses (*SI Appendix*, Fig. S10*A*) and the pregnant *Dnase1l3*$^{-/-}$ mice carrying *Dnase1l3*$^{-/-}$ fetuses (*SI Appendix*, Fig. S10*B*). The fetal DNA molecules were consistently found to be shorter than maternal DNA molecules. These findings were consistent with those of the nonpregnant model in which an increase in the frequencies of both short (<120 bp) and long (>250 bp) DNA molecules was observed in *Dnase1l3*$^{-/-}$ mothers compared with WT (*Dnase1l3*$^{+/+}$) mice (*SI Appendix*, Fig. S11). Thus, the aberrant size of plasma DNA in *Dnase1l3*-deficient dams cannot be rescued by the presence of DNASE1L3 in the fetus.

Plasma DNA End Motifs in Pregnant Mice. The murine pregnancy model provided an opportunity to investigate if the contribution of DNASE1L3 to the fragmentation of plasma DNA might occur at a systemic level (e.g., through DNASE1L3 activity in plasma) or at a tissue level (e.g., within the placenta). Hence, for a pregnancy involving a *Dnase1l3*$^{-/-}$ female pregnant mouse carrying *Dnase1l3*$^{+/-}$ fetuses, the pregnant mother did not express DNASE1L3 whereas the fetuses would be expected to express DNASE1L3, albeit at a lower level than *Dnase1l3*$^{+/+}$ fetuses. If the *Dnase1l3*$^{+/-}$ fetuses could release DNASE1L3 into the circulation of their *Dnase1l3*$^{-/-}$ pregnant mother, then one would expect that there might be a partial reversal of the phenotype associated with *Dnase1l3* deletion in the pregnant mother.

We pursued this question of phenotype reversal based on the six highest-ranked plasma DNA end motifs associated with *Dnase1l3* deletion described above. Fig. 6 illustrates the reduction in plasma DNA fragments with these six highest-ranked end motifs in nonpregnant *Dnase1l3*$^{-/-}$ mice compared with WT (*Dnase1l3*$^{+/+}$) mice. Pregnancies involving pregnant mothers and fetuses that were both *Dnase1l3*$^{+/+}$ had plasma DNA end-motif frequencies that were similar to those of the nonpregnant WT mice. Using the strain difference between the pregnant mothers (i.e., B6) and the impregnating males (i.e., BALB/c), we were able to separately analyze the end-motif frequencies of plasma DNA fragments derived from the fetuses and the pregnant mothers. Hence, plasma DNA fragments with BALB/c genetic signatures were derived from the fetuses while plasma DNA fragments with B6 genetic signatures were derived predominantly from the mother, with a small proportion contributed by the fetuses. Using fetal DNA fragments, we could also calculate the percentage of fetal DNA that was present in the maternal plasma. Using the percentage of fetal DNA in maternal plasma, we mathematically adjusted the plasma DNA motif frequencies for the circulating DNA of B6 background such that they represented just those contributed by the pregnant mother, but excluding those contributed by the fetuses [under the heading "(adjusted)" in Fig. 6]. As fetal DNA represented a minority population in maternal plasma, the effect of such an adjustment was relatively minor.

For pregnancies involving *Dnase1l3*$^{-/-}$ pregnant mice and *Dnase1l3*$^{+/-}$ fetuses, we observed that the frequencies of the six highest-ranked plasma DNA end motifs were in between those of

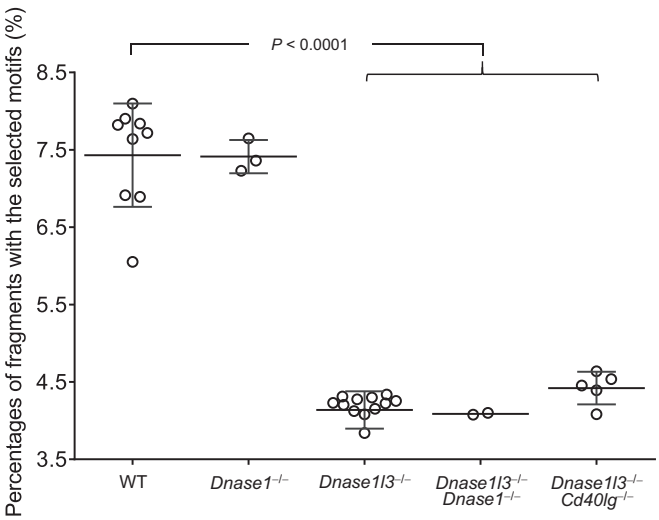

Fig. 3. Percentages of plasma DNA fragments with the selected motifs among groups. The select motifs CCCA, CCTG, CCAG, CCAA, CCAT, and CCTC are the top six 4-mer motifs ranked with the highest frequencies in the WT group and show a statistically significant reduction in *Dnase1l3*$^{-/-}$ mice. Samples from 9 WT mice, 3 *Dnase1*$^{-/-}$ mice, 13 *Dnase1l3*$^{-/-}$ mice, 2 *Dnase1*$^{-/-}$/*Dnase1l3*$^{-/-}$ mice, and 5 *Dnasell3*$^{-/-}$/*Cd40lg*$^{-/-}$ mice were sequenced. Each circle represents one mouse. Statistical difference in the percentage between WT mice and mice with *Dnase1l3* deletion was calculated by using the Wilcoxon rank-sum test.

Table 2. Characteristics of the pregnant mice

Case no.	Maternal genome background	Maternal *Dnase1l3* genotype	Age, wk	Approximate days of pregnancy	Fetal genome background	Fetal *Dnase1l3* genotype	No. of fetuses	Fetal percentage*, %
Mu31	B6	+/+	12.0	15	B6, BALB/c	+/+	7	6.4
Mu45	B6	+/+	10.9	18	B6, BALB/c	+/+	8	8.4
Mu46	B6	–/–	11.4	18	B6, BALB/c	+/–	6	20.7
Mu47	B6	–/–	28.1	16	B6, BALB/c	+/–	8	15.1
Mu48	B6	–/–	11.3	16	B6, BALB/c	+/–	5	11.6
Mu49	B6	–/–	11.3	17	B6, BALB/c	+/–	4	11.4
Mu104	B6	–/–	34.4	17	B6	–/–	9	12.3
Mu105	B6	–/–	17.6	16	B6	–/–	8	14.9
Mu106	B6	–/–	38.6	16	B6	–/–	8	12.8

*The fetal percentages in a pregnant mouse carrying fetuses with the B6 and BALB/c genomic background were deduced using a SNP-based approach. The fetal percentages in a pregnant mouse carrying fetuses with the B6 genomic background (i.e., Mu104, Mu105, and Mu106) were estimated using reads aligned to the Y chromosome.

the nonpregnant *Dnase1l3*$^{+/+}$ and nonpregnant *Dnase1l3*$^{-/-}$ mice. The pregnant *Dnase1l3*$^{-/-}$ mice showed a 1.23-fold increase in the six highest-ranked plasma DNA end motifs compared with nonpregnant *Dnase1l3*$^{-/-}$ mice. These results suggested the presence of a systemic effect within the pregnant mothers' plasma due to DNASE1L3 produced by the *Dnase1l3*$^{+/-}$ fetuses.

We also observed that the frequencies of the six highest-ranked plasma DNA end motifs in the plasma DNA derived from the *Dnase1l3*$^{+/-}$ fetuses were higher than those derived from the pregnant mother ($P = 0.0286$, Wilcoxon rank-sum test). This observation suggested that in addition to a systemic effect in the pregnant mother's body there was also a local effect of DNASE1L3 produced by the *Dnase1l3*$^{+/-}$ fetuses on fetal DNA (e.g., within the placenta). It is interesting to note that the fetal DNA subset in the plasma of pregnant *Dnase 1l3*$^{-/-}$ mice carrying *Dnase1l3*$^{+/-}$ fetuses showed an average of 18.3% reduction in the end motifs compared with the fetal subset of those carrying *Dnase1l3*$^{+/+}$ fetuses. This observation suggests that there might be a local DNASE1L3 effect within placental cells.

Discussion

In this work, we demonstrated that *Dnase1l3*$^{-/-}$ mice exhibited a number of specific aberrations in the fragmentation of plasma DNA. First, we observed an increase in the amount of longer DNA molecules, especially in the di-, tri-, and tetranucleosomal sizes (*SI Appendix*, Fig. S1). DNA sequencing analyses also confirmed these results for the di- and trinucleosomal-sized fragments (Fig. 1). Due to the inefficiency of the Illumina platform in sequencing DNA molecules >600 bp, we did not plot sequencing data above that size in Fig. 1*B*. Second, there was a 40% increase in the amount of short plasma DNA molecules below 120 bp (Fig. 1*C* and *SI Appendix*, Fig. S3). There was a positive correlation between the amount of short DNA and anti-dsDNA antibody levels (*SI Appendix*, Fig. S5*A*). *Dnase1l3*$^{-/-}$ mice are prone to develop antibodies to chromatin and DNA and a SLE-like syndrome (20, 26). Furthermore, an increase in the amounts of short plasma DNA molecules was also observed in human subjects with SLE (21). We proposed that this increase in the amounts of short plasma DNA was related to such autoantibodies. Our hypothesis is supported by a reduction in the amounts of short plasma DNA in *Dnase1l3*$^{-/-}$/*Cd40lg*$^{-/-}$ mice that failed to develop autoantibody response (*SI Appendix*, Fig. S4).

We hypothesized that there might be DNA motifs that DNASE1L3 might preferentially cleave. If such DNA motifs existed and if DNASE1L3 was one of the enzymes involved in the fragmentation of DNA that eventually was found in plasma, we conjectured that such DNA motifs should be present at relatively high levels in the plasma of WT mice and would be reduced in *Dnase1l3*$^{-/-}$ mice. Indeed, we found a number of such motifs (Table 1), the top six of which all started with CC. These results were consistent with the observations of Chandrananda et al. (27), who observed an overrepresentation of CC at the ends of plasma DNA sequenced from human pregnant women. Our data suggest that DNASE1L3 may contribute to this phenomenon.

One actively pursued area in the field of circulating fetal DNA involves the use of circulating fetal DNA in maternal plasma for noninvasive prenatal testing (1, 2). It has been known for a number of years that circulating fetal DNA molecules have a size distribution that is shorter than their maternal counterparts (5, 8, 9). Paired-end massively parallel sequencing enables high-resolution measurement of DNA size at single-base resolution by measuring the number of nucleotides between the ends of the sequenced fragment. Using paired-end sequencing, circulating fetal and maternal DNA molecules have been shown to have peak frequencies at 143 bp and 166 bp, respectively (5). Indeed, such a subtle difference in the size between maternal and fetal DNA has already been used in noninvasive prenatal diagnostics (9, 14).

Considering that the Illumina platform has not been designed to sequence molecules >600 bp, we used the single-molecule, real-time sequencing platform from Pacific Biosciences to further sequence two cases from each of the groups. This platform was designed to generate DNA sequences in the kilobases range (24, 25). Using the Pacific Biosciences platform, we were able to analyze plasma DNA reads well into the 1,500-bp range, and

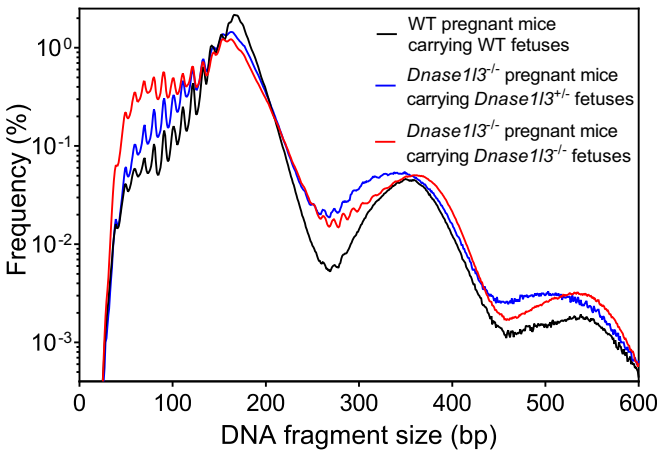

Fig. 4. Mean size distributions of plasma DNA fragments in pregnant mice. Solid black line represents data from two pregnant WT mice carrying WT fetuses. Solid blue line represents data from four pregnant *Dnase1l3*$^{-/-}$ mice carrying *Dnase1l3*$^{+/-}$ fetuses. Solid red line represents data from three pregnant *Dnase1l3*$^{-/-}$ mice carrying *Dnase1l3*$^{-/-}$ fetuses.

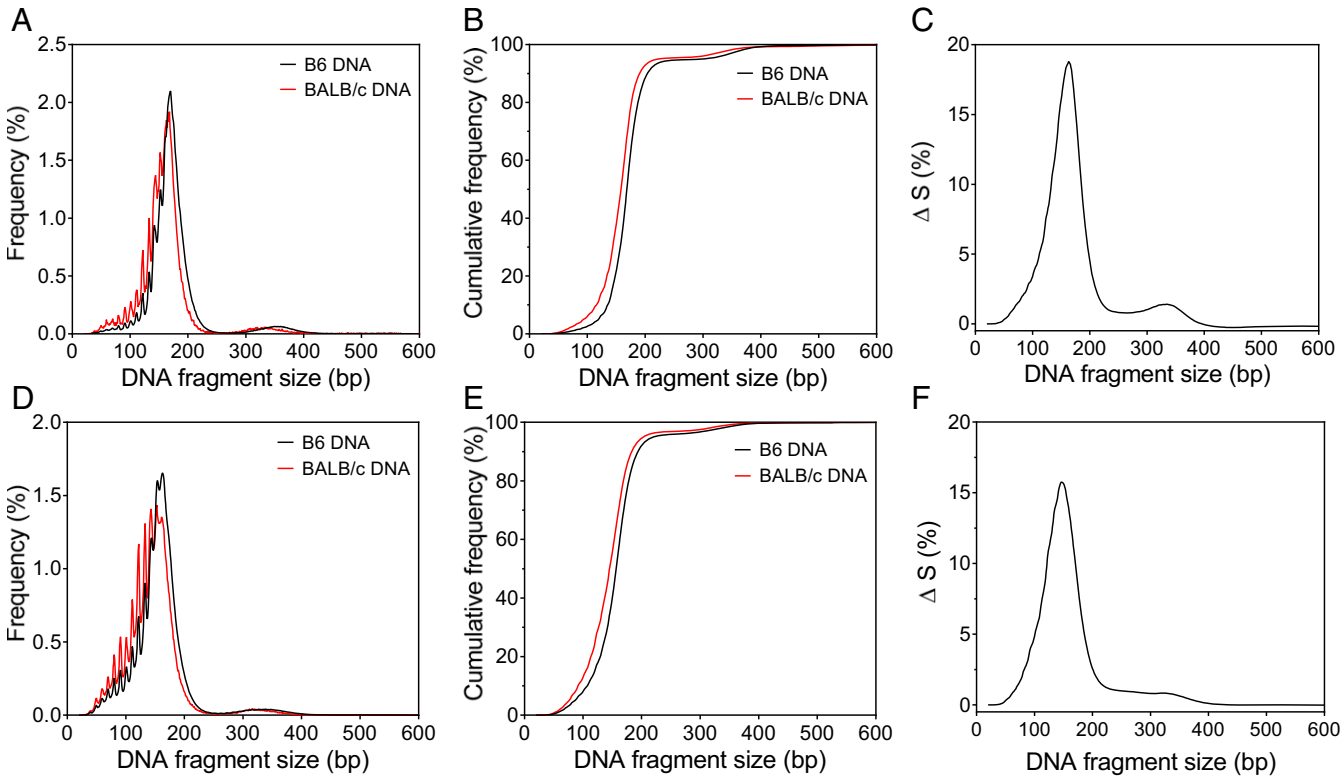

Fig. 5. Difference between maternal and fetal DNA size profiles. (*A*) Size distributions, (*B*) plot of cumulative size frequencies for maternal DNA (black) and fetal DNA (red), and (*C*) the difference in cumulative frequencies, denoted as ΔS, between maternal and fetal DNA for a representative WT pregnant mouse (Mu31). (*D*) Size distributions, (*E*) plot of cumulative frequencies of plasma DNA size for maternal DNA (black) and fetal DNA (red), and (*F*) the difference in cumulative frequencies, denoted as ΔS, between maternal and fetal DNA for a representative *Dnase1l3*$^{-/-}$ pregnant mouse (Mu47).

occasionally at close to 2,000 bp. However, such long molecules were present at very low frequencies with the average percentage of DNA molecules from 600 bp to 2,000 bp in size for WT and *Dnase1l3*$^{-/-}$ mice being present at 0.5% and 2.1%, respectively (*SI Appendix*, Fig. S6). Most significantly, the relative size distributions of plasma DNA fragments for mice with WT or knockout genotypes as observed using the Pacific Biosciences platform were consistent with those observed using the Illumina platform (Fig. 1). Since the long plasma DNA molecules above 600 bp in size only represented less than 5% in the sequences obtained by the Pacific Biosciences platform, these results suggest that sequencing data generated using the Illumina platform had already captured the size profile of most of the plasma DNA molecules in our experimental system. Hence, for subsequent analyses, we focused only on the Illumina platform.

From our data, there was no statistically significant difference in both short (<120 bp) and long (>250 bp) DNA between pregnant *Dnase1l3*$^{-/-}$ mice carrying *Dnase1l3*$^{+/-}$ fetuses and nonpregnant *Dnase1l3*$^{-/-}$ mice (long, $P = 0.33$; short, $P = 0.85$; Wilcoxon rank-sum test; *SI Appendix*, Fig. S11). We concluded that pregnant *Dnase1l3*$^{-/-}$ mice carrying *Dnase1l3*$^{+/-}$ fetuses had an overall size distribution of plasma DNA that was similar to nonpregnant *Dnase1l3*$^{-/-}$ mice. In particular, such pregnancies maintained the relative size shortening of fetal DNA molecules in maternal plasma, compared with their maternal counterparts.

However, using the plasma DNA end motif preference data (Table 1), one could further obtain insights into the site of action of DNASE1L3. Hence, in pregnancies in which the pregnant mothers were *Dnase1l3*$^{-/-}$ and the fetuses were *Dnase1l3*$^{+/-}$, one would expect that the mothers would not be able to produce DNASE1L3 while the fetuses would still be able to produce DNASE1L3. If the fetally produced DNASE1L3 enzyme was able to gain access into the maternal circulation and acted systematically, then one would observe a partial normalization of the six highest-ranked motifs in plasma DNA molecules. This was indeed observed from the data shown in Fig. 6 in which plasma DNA molecules of B6 origin (mainly of maternal origin) exhibited a partial normalization of the DNASE1L3-preferred end motifs toward the levels observed in WT mice. Because the majority of plasma DNA was derived from hematopoietic cells and the DNASE1L3 in this setting was derived from the fetus, these data suggested that DNASE1L3 might mediate plasma DNA fragmentation in a cell-extrinsic manner.

It is also notable that, for each of the six DNASE1L3-preferred end motifs, the degree of normalization of the circulating BALB/c DNA in maternal plasma, which was all fetally derived, was higher than that of circulating B6 DNA (which was predominantly of maternal origin) (*SI Appendix*, Fig. S12 *A*–*F*). This observation suggests that there might be a higher activity of the DNASE1L3 enzyme at the site of its production from the fetuses. As fetal DNA in maternal plasma in humans has been shown to be derived from the placenta (28, 29), one site of action of the fetally derived DNASE1L3 might be in the placenta. This possibility is supported by recent data from a mouse cell atlas project in which *Dnase1l3* gene expression has indeed been found in the murine placenta (30).

Our work reported here has demonstrated that DNASE1L3 plays a role in the fragmentation of plasma DNA. It is likely that there might be other players in this fragmentation process. It would thus be of value to investigate the role of other nucleases in this process. In this regard, we had previously demonstrated deleting the *Dnase1* gene in mouse did not appear to alter the length of circulating DNA (17). In the present work, our data suggest that deleting both the *Dnase1* and *Dnase1l3* genes together appears to increase the amount of short DNA below 120 bp (Fig. 1*C*). This

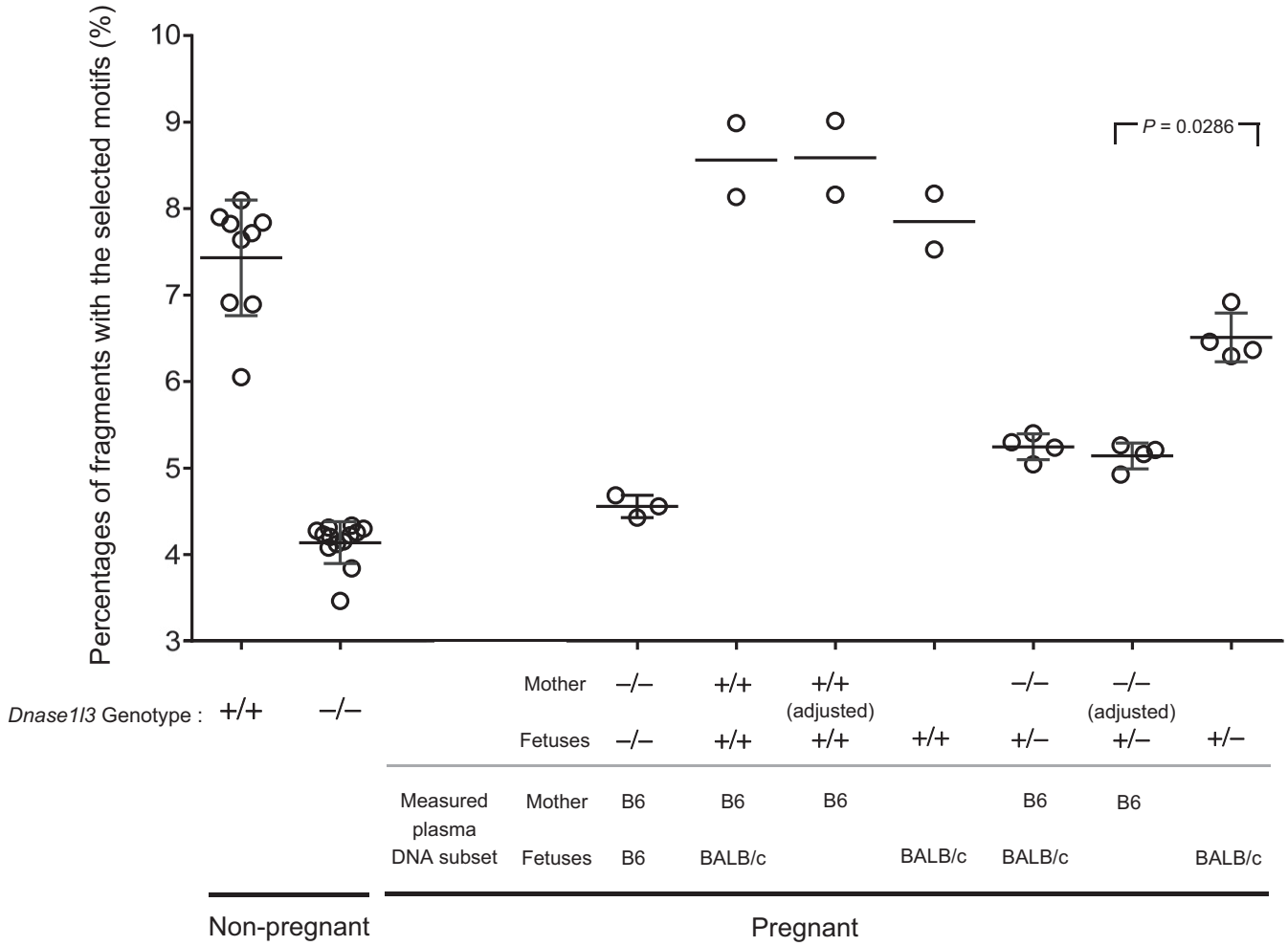

Fig. 6. Percentages of fragments with the six selected motifs, including CCCA, CCTG, CCAG, CCAA, CCAT, and CCTC, in plasma DNA of nonpregnant mice; maternal and fetal DNA fractions in plasma of pregnant mice with different *Dnase1l3* genotypes. Each circle represents the data from one mouse. The genotypes of the nonpregnant mice as well as the fetal and maternal DNA subset of pregnant mice are annotated under the *x* axis. The first two groups are nonpregnant WT and *Dnase1l3*$^{-/-}$ mice, respectively. For pregnant mice, the strains of the maternal and fetal DNA subset in plasma are also annotated. B6 and BALB/c are two different mouse strains with different genetic backgrounds. As the motifs of fetal DNA sequences would theoretically affect the measurement of motifs in the shared sequences, the abundance of a motif from maternally derived sequences was adjusted by the fetal DNA fraction as described in *Materials and Methods*. The adjusted percentages of the selected motifs of the maternal DNA subset are labeled with "(adjusted)" on the *x* axis. Statistical difference in the percentage between maternal and fetal DNA subsets of pregnant mice with *Dnase1l3* deletion was calculated by using the Wilcoxon rank-sum test.

observation would require further confirmation and exploration in future work. It is also possible that the loss of DNASE1 enzymatic function, either on its own or in conjunction with DNASE1L3, might result in aberrations of circulating DNA that are not seen with the techniques used in the present work. We would continue to explore if DNASE1L3 and DNASE1 may work synergistically on DNA fragmentation (31). Further work using other sequencing platforms, such as nanopore sequencing (32), might be used to explore this issue. It would also be interesting to further explore the *Dnase1* deletion mouse model in the pregnancy context, as has been done for *Dnase1l3* in the present work and in other experimental systems, for example sepsis (33).

Homozygous mutations of the *DNASE1L3* gene in humans have been described to be associated with SLE, often preceded by hypocomplementemic urticarial vasculitis syndrome (34–36). It would be interesting to see if the plasma DNA aberrations observed in the mouse models described in this paper can also be seen in these human subjects. It also remains to be examined how the observed lengthening of circulating DNA is related to the increased DNA load of circulating microparticles in DNASE1L3-deficient patients and experimental animals (20), and how it may contribute to the breach of tolerance and anti-DNA responses in these conditions.

In the present study, it is intriguing that the plasma DNA aberrations observed in the mice with the deletion of *Dnase1l3* only accounted for a small proportion of circulating DNA molecules (<10%). We postulated that DNASE1L3 may only be one of a number of nucleases that are involved in the homeostasis of circulating DNA. To identify these additional players in fragmentation mechanisms, further studies using the experimental approach described in this work might be a fruitful avenue of research.

In summary, we have demonstrated that deletion of the *Dnase1l3* gene in mice was associated with aberrations in plasma DNA fragmentation. These results suggested that DNASE1L3 was one of the components of the mechanism for generating circulating DNA fragments. We believe that it would be a productive direction of research to explore the effects of other nucleases in the characteristics of circulating nucleic acids. An enhanced understanding of the biology of circulating DNA might help us to design optimal strategies for their use in molecular diagnostics.

Materials and Methods

Animals. All animal studies were performed according to the investigator's protocol approved by the Institutional Animal Care and Use Committees of New York University School of Medicine. The *Dnase1l3*$^{-/-}$ mouse model on C57BL/6 (B6) background [*Dnase1l3*$^{LacZ/LacZ}$] was described previously (20). Mice carrying a targeted allele of *Dnase1* (*Dnase1*$^{tm1.1(KOMP)Vlcg}$) on B6 background were obtained from the Knockout Mouse Project and crossed with WT B6 and *Dnase1l3*$^{-/-}$ mice to obtain *Dnase1*$^{-/-}$ and *Dnase1*$^{-/-}$/*Dnase1l3*$^{-/-}$ mice, respectively. Mice carrying a targeted allele of *Cd40lg* [B6.129S2-*Cd40lg*^{tm1Imx}/J] on B6 background were obtained from the The Jackson Laboratory and crossed to obtain *Dnase1l3*$^{-/-}$/*Cd40lg*$^{-/-}$ mice. WT control mice of B6 background were bred in the same animal facility or purchased from Taconic, Inc. and maintained in the same facility. WT mice of BALB/c background for the pregnancy studies were obtained from Taconic, Inc. Pregnant dams were killed and exsanguinated for plasma collection, and pregnancy terms were estimated by embryo morphology.

Sample Processing and DNA Extraction. Animals were killed and exsanguinated by cardiac puncture. Blood was transferred into EDTA-containing collection tubes. The blood samples were first centrifuged at 1,600 × *g* for 10 min at 4 °C. The plasma portion was further subjected to centrifugation at 16,000 × *g* for 10 min at 4 °C to pellet the residual cells and platelets. The resulting plasma was harvested. Circulating cell-free DNA was extracted from 0.2 to 0.5 mL of plasma using the DSP Blood Mini Kit (Qiagen) as previously described (37).

DNA Library Preparation and Electrophoresis. Circulating DNA libraries were constructed by using the KAPA HTP Library Preparation Kit (Roche) and purified using a MinElute Reaction Cleanup Kit (Qiagen) according to the manufacturer's instructions. Adaptor-ligated libraries were analyzed on an Agilent 4200 TapeStation (Agilent Technologies) using the High Sensitivity D1000 ScreenTape System (Agilent Technologies) for quality control and gel-based size determination. Before sequencing, the libraries were quantified by qPCR using a KAPA Library Quantification Kit (Roche) on a LightCycler 96 instrument (Roche).

DNA Sequencing Using the Illumina Platform. The DNA libraries were sequenced for 75 bp for each end in a paired-end format on a NextSeq. 500 instrument (Illumina). Real-time image analysis and base calling were performed using the NextSeq Control Software v2.1.0 and Real Time Analysis Software v2.4.11 (Illumina). After base calling, adapter sequences and low quality bases (i.e., quality score < 5) on the 3′ ends of the reads were removed.

For the analysis of sequencing data, the sequenced reads were aligned to the non-repeat-masked mouse reference genome (NCBI build 37/UCSC mm9) using the Short Oligonucleotide Alignment Program 2 as previously described (37, 38). Only paired-end reads which were aligned to the same chromosome in a correct orientation with an insert size less than 5,000 bp were used for downstream analysis. For paired-end reads sharing the same start and end aligned genomic coordinates only one would be kept for further analysis, while the rest were deemed to be PCR duplicates and were discarded. *SI Appendix*, Table S1 summarizes the number of sequenced fragments of each sample detected by using the Illumina platform.

DNA Sequencing Using the Pacific Biosciences Sequencing Platform. Sequencing templates were constructed using SMRTbell Template Prep Kit 1.0 - SPv3 (Pacific Biosciences) according to the manufacturer's instructions, except that the amplicon templates were purified with AMPure PB beads (Pacific Biosciences). Sequencing primer annealing and polymerase binding conditions were calculated with SMRT Link v5.1.0 software (Pacific Biosciences). Briefly, sequencing primer v3 was annealed to sequencing template, then polymerase was bound to templates using Sequel Binding and Internal Control Kit 2.1 (Pacific Biosciences). Sequencing was performed on a Sequel SMRT Cell 1M v2 for each template. Each sequencing movie was collected on the Sequel system for 10 h with Sequel sequencing kit 2.1 (Pacific Biosciences).

Molecular Size Determination of Circulating DNA. Following paired-end sequencing, both end sequences of each DNA molecule were aligned to the mouse reference genome for the B6 strain (NCBI build 37/UCSC mm9). The genome coordinates of the aligned ends were then used to deduce the sizes of the sequenced DNA molecules (8). *SI Appendix*, Table S2 summarizes the percentage and number of long DNA molecules detected using the Illumina and the Pacific Biosciences sequencing platforms.

Motif Analysis of Circulating DNA. To study whether deletion of the *Dnase1l3* gene would alter the cleavage pattern of circulating DNA, the first 4-bp sequence (i.e., a 4-mer motif) on each 5′ fragment end of plasma DNA molecules was determined. The frequency of each of the 256 possible motifs (i.e., 4 × 4 × 4 × 4) was calculated and normalized by the total number of ends. For each motif, the difference in the frequency between *Dnase*1l3$^{-/-}$ mice and WT mice was tested by the Wilcoxon rank-sum test and its *P* value was adjusted by the Holm–Bonferroni procedure because of multiple comparisons (39).

Size and Motif Analyses for Pregnancy Model Involving both the B6 and BALB/c Genetic Backgrounds. The female *Dnase1l3*$^{-/-}$ and WT (*Dnase1l3*$^{+/+}$) mice of the B6 genetic background were impregnated by male WT (*Dnase1l3*$^{+/+}$) mice of the BALB/c genetic background. Hence, their fetuses would inherit the SNP signatures of the B6 (mother) and BALB/c (father) strains. The maternal plasma DNA of a pregnant B6 mouse was composed of molecules from both the maternal B6 genome and the paternal BALB/c genome. In the bioinformatics data analysis, the paired-end reads from plasma DNA of pregnant mice were initially aligned to the B6 reference genome.

Based on the alignment results, the sequenced fragments bearing the paternal-specific variants (i.e., fetal DNA molecules) were identified using the 4,991,500 SNPs that were different between B6 and BALB/c strains, which were annotated in the Mouse Genomes Project (https://www.sanger.ac.uk/science/data/mouse-genomes-project). Since there were a number of non-single nucleotide genetic differences between the two strains, for example small insertions/deletions and copy number variations, the genomic coordinates of the two strains were not consistent. Hence, the accuracy in determining fragment sizes and motifs would be affected when analyzing BALB/c sequences using the B6 genome as a reference. To overcome this issue, DNA fragments carrying the paternal-specific variants were realigned to the BALB/c reference genome and the actual fragment size of fetal DNA molecules was determined based on the realigned genomic coordinates. The motifs of fetal DNA molecules were also deduced from realigned results in the BALB/c reference genome. However, the plasma DNA molecules bearing the shared variants would generally reflect the maternal characteristics because the majority of those molecules were likely derived from B6 maternal hematopoietic cells. Thus, for those DNA fragments carrying shared alleles, the fragment size and motif analyses were performed directly using paired-end reads aligned to the B6 reference genome.

The fetal DNA fraction (F) was calculated by using the following formula:

$$F = \frac{2p}{p+q} \times 100\%,$$

where p is the number of sequenced reads carrying fetal-specific variants and q is the number of sequenced reads carrying variants shared by the mother and the fetuses.

Motif Correction for Shared Sequences in Pregnant Mice Involving both the B6 and BALB/c Genetic Backgrounds. We analyzed the motifs derived from maternal and fetal sequences, the plasma DNA fragments carrying the informative SNPs, in which the maternal and paternal genotypes were both homozygous but for a different variant each. In this scenario, the maternal and paternal genotypes could be denoted by AA and BB, respectively, making the fetal genotype AB. There was a small proportion of fetal DNA fragments contributing to those shared sequences carrying variants of A.

The motifs of fetal DNA sequences would theoretically affect the measurement of motifs in the shared sequences. Thus, to infer the abundance of a motif present in maternally derived sequences, we needed to adjust the abundance of motifs of maternal sequences according to the fetal DNA fraction (*f*). Assuming that the observed motifs abundance (*M*) in shared sequences was a linear combination of motifs contributed by the maternally derived sequences (M_1) and the fetally derived sequences (M_2), respectively, we derived the following formula:

$$M_1 \times (1-P) + M_2 \times P = M, \quad [1]$$

where *P* was the percentage of shared sequences released by the fetuses, which was

$$P = \frac{f}{2-f}.$$

Thus, M_1 could be deduced according to Eq. **1**:

$$M_1 = \frac{2M - (M+M_2) \times f}{2-2f}. \quad [2]$$

M_1 was the abundance of a motif in shared sequences adjusted by the fetal DNA fraction and would thus correctly reflect the motifs derived from maternal-derived sequences.

Size and Motif Analyses of Pregnancy Model Involving only the B6 Genetic Background. To test whether physiological changes in pregnancy would confound the motif analysis, we allowed three *Dnase1l3*$^{-/-}$ B6 females to mate with the *Dnase1l3*$^{-/-}$ B6 males, resulting in pregnancies carrying *Dnase1l3*$^{-/-}$ fetuses of the B6 background. Fetal DNA reads were taken as those aligned to the Y chromosome, which were originated from the male fetuses. The size analysis of the fetal DNA was performed using such Y chromosome-aligned reads. As both the maternal and fetal DNA was of B6 background, the motif analysis of these three pregnant mice was the same as that for the nonpregnant mice.

Quantification of Anti-dsDNA IgG Antibodies. Plasma was obtained from mice using the same protocol as described above. Anti-dsDNA IgG titers were determined by ELISA using plates precoated with poly-L-lysine (0.01% wt/vol in PBS) for 1 h at room temperature and then coated with 0.01 mg/mL calf thymus DNA as an antigen. After incubation with plasma, the amount of bound IgG was measured with an alkaline phosphatase-conjugated goat anti-mouse IgG antibody (1:1,000; Jackson Immunoresearch). Antigen-specific IgG levels were determined using serial dilutions of the plasma from a positive animal as a standard and expressed as units per milliliter.

Statistical Analysis. Analysis was performed using custom-built programs written in Perl and R languages. Statistical difference was calculated using the Wilcoxon rank-sum test unless otherwise specified. A *P* value of less than 0.05 was considered as statistically significant and all probabilities were two-tailed.

ACKNOWLEDGMENTS. This work was supported by the Research Grants Council of the Hong Kong SAR Government under Theme-Based Research Scheme T12-403/15-N; the Colton Center for Autoimmunity; the Lupus Research Alliance; and NIH Grants AR071703, AR070591, GM007308, and AI100853. Y.M.D.L. is supported by an endowed chair from the Li Ka Shing Foundation.

1. Lo YMD, et al. (1997) Presence of fetal DNA in maternal plasma and serum. *Lancet* 350:485–487.
2. Chiu RWK, et al. (2008) Noninvasive prenatal diagnosis of fetal chromosomal aneuploidy by massively parallel genomic sequencing of DNA in maternal plasma. *Proc Natl Acad Sci USA* 105:20458–20463.
3. Chan KCA, et al. (2017) Analysis of plasma Epstein-Barr virus DNA to screen for nasopharyngeal cancer. *N Engl J Med* 377:513–522.
4. Cohen JD, et al. (2018) Detection and localization of surgically resectable cancers with a multi-analyte blood test. *Science* 359:926–930.
5. Lo YMD, et al. (2010) Maternal plasma DNA sequencing reveals the genome-wide genetic and mutational profile of the fetus. *Sci Transl Med* 2:61ra91.
6. Snyder MW, Kircher M, Hill AJ, Daza RM, Shendure J (2016) Cell-free DNA comprises an in vivo nucleosome footprint that informs its tissues-of-origin. *Cell* 164:57–68.
7. Ulz P, et al. (2016) Inferring expressed genes by whole-genome sequencing of plasma DNA. *Nat Genet* 48:1273–1278.
8. Chan KCA, et al. (2004) Size distributions of maternal and fetal DNA in maternal plasma. *Clin Chem* 50:88–92.
9. Yu SCY, et al. (2014) Size-based molecular diagnostics using plasma DNA for noninvasive prenatal testing. *Proc Natl Acad Sci USA* 111:8583–8588.
10. Jiang P, et al. (2015) Lengthening and shortening of plasma DNA in hepatocellular carcinoma patients. *Proc Natl Acad Sci USA* 112:E1317–E1325.
11. Underhill HR, et al. (2016) Fragment length of circulating tumor DNA. *PLoS Genet* 12: e1006162.
12. Sun K, et al. (2018) Size-tagged preferred ends in maternal plasma DNA shed light on the production mechanism and show utility in noninvasive prenatal testing. *Proc Natl Acad Sci USA* 115:E5106–E5114.
13. Sun K, et al. (2017) COFFEE: Control-free noninvasive fetal chromosomal examination using maternal plasma DNA. *Prenat Diagn* 37:336–340.
14. Cirigliano V, Ordoñez E, Rueda L, Syngelaki A, Nicolaides KH (2017) Performance of the neoBona test: A new paired-end massively parallel shotgun sequencing approach for cell-free DNA-based aneuploidy screening. *Ultrasound Obstet Gynecol* 49: 460–464.
15. Mouliere F, et al. (2011) High fragmentation characterizes tumour-derived circulating DNA. *PLoS One* 6:e23418.
16. Lam WKJ, et al. (2018) Sequencing-based counting and size profiling of plasma Epstein-Barr virus DNA enhance population screening of nasopharyngeal carcinoma. *Proc Natl Acad Sci USA* 115:E5115–E5124.
17. Cheng THT, et al. (2018) DNase1 does not appear to play a major role in the fragmentation of plasma DNA in a knockout mouse model. *Clin Chem* 64:406–408.
18. Napirei M, Ludwig S, Mezrhab J, Klöckl T, Mannherz HG (2009) Murine serum nucleases–contrasting effects of plasmin and heparin on the activities of DNase1 and DNase1-like 3 (DNase1l3). *FEBS J* 276:1059–1073.
19. Mizuta R, et al. (2006) Action of apoptotic endonuclease DNase gamma on naked DNA and chromatin substrates. *Biochem Biophys Res Commun* 345:560–567.
20. Sisirak V, et al. (2016) Digestion of chromatin in apoptotic cell microparticles prevents autoimmunity. *Cell* 166:88–101.
21. Chan RWY, et al. (2014) Plasma DNA aberrations in systemic lupus erythematosus revealed by genomic and methylomic sequencing. *Proc Natl Acad Sci USA* 111: E5302–E5311.
22. Renshaw BR, et al. (1994) Humoral immune responses in CD40 ligand-deficient mice. *J Exp Med* 180:1889–1900.
23. Xu J, et al. (1994) Mice deficient for the CD40 ligand. *Immunity* 1:423–431.
24. Nattestad M, et al. (2018) Complex rearrangements and oncogene amplifications revealed by long-read DNA and RNA sequencing of a breast cancer cell line. *Genome Res* 28:1126–1135.
25. Pollard MO, Gurdasani D, Mentzer AJ, Porter T, Sandhu MS (2018) Long reads: Their purpose and place. *Hum Mol Genet* 27:R234–R241.
26. Weisenburger T, et al. (2018) Epistatic interactions between mutations of deoxyribonuclease 1-like 3 and the inhibitory Fc gamma receptor IIB result in very early and massive autoantibodies against double-stranded DNA. *Front Immunol* 9:1551.
27. Chandrananda D, Thorne NP, Bahlo M (2015) High-resolution characterization of sequence signatures due to non-random cleavage of cell-free DNA. *BMC Med Genomics* 8:29.
28. Chim SS, et al. (2005) Detection of the placental epigenetic signature of the maspin gene in maternal plasma. *Proc Natl Acad Sci USA* 102:14753–14758.
29. Sun K, et al. (2015) Plasma DNA tissue mapping by genome-wide methylation sequencing for noninvasive prenatal, cancer, and transplantation assessments. *Proc Natl Acad Sci USA* 112:E5503–E5512.
30. Han X, et al. (2018) Mapping the mouse cell atlas by microwell-seq. *Cell* 172: 1091–1107.e17.
31. Koyama R, et al. (2016) DNase γ, DNase I and caspase-activated DNase cooperate to degrade dead cells. *Genes Cells* 21:1150–1163.
32. Cheng SH, et al. (2015) Noninvasive prenatal testing by nanopore sequencing of maternal plasma DNA: Feasibility assessment. *Clin Chem* 61:1305–1306.
33. Jiménez-Alcázar M, et al. (2017) Host DNases prevent vascular occlusion by neutrophil extracellular traps. *Science* 358:1202–1206.
34. Al-Mayouf SM, et al. (2011) Loss-of-function variant in DNASE1L3 causes a familial form of systemic lupus erythematosus. *Nat Genet* 43:1186–1188.
35. Carbonella A, et al. (2017) An autosomal recessive DNASE1L3-related autoimmune disease with unusual clinical presentation mimicking systemic lupus erythematosus. *Lupus* 26:768–772.
36. Ozçakar ZB, et al. (2013) DNASE1L3 mutations in hypocomplementemic urticarial vasculitis syndrome. *Arthritis Rheum* 65:2183–2189.
37. Chiu RWK, et al. (2011) Non-invasive prenatal assessment of trisomy 21 by multiplexed maternal plasma DNA sequencing: Large scale validity study. *BMJ* 342:c7401.
38. Li R, et al. (2009) SOAP2: An improved ultrafast tool for short read alignment. *Bioinformatics* 25:1966–1967.
39. Benjamini Y, Hochberg Y (1995) Controlling the false discovery rate: A practical and powerful approach to multiple testing. *J R Stat Soc B* 57:289–300.